Performance of an Iron Aluminide Metal Filter in a Reducing Environment

V.J. Novick, R.K. Ahluwalia, K. Natesan, W.K. Soppet, and B.E. Spencer

(Submitted 5 December 2000; in revised form 23 March 2001)

A laboratory-scale apparatus has been used for unattended, long duration, continuous, flow-through testing of an iron aluminide sintered metal filter under reducing conditions. Two candle specimens were exposed for 1009 to 2251 h to 600 °C gas containing 5% CO, 11% H_2, 12% CO_2, 12% H_2O, 60% N_2, 0.5% H_2S, 2.4 ppmv NaCl, 4.7 ppmv KCl, 26.1 ppmv HCl, and 5530 ppmw ash from a transport reactor operated in gasification mode. A database was established on pressure drop of the as-received and exposed filter as a function of face velocity and temperature. Tests were conducted to investigate the effects of back pulse parameters on filter regenerability. Results are reported on the critical reservoir pressure and pulse duration for maintaining a stable saw-tooth profile of pressure drop across the filter element. Data are obtained to characterize the effect of chemical and thermal aging on tensile strength, fast fracture strength, and microstructure.

Keywords aluminides, coal gasification filters, Fe-28% Al-5% Cr, fracture toughness, high temperature

Introduction

Porous iron aluminides (Fe_3Al) are being evaluated for high-temperature filtration applications in advanced pressurized fluidized bed and integrated gasification combined cycle plant applications. In laboratory tests, the iron aluminide alloy has shown higher resistance to sulfidation when exposed to hydrogen sulfide and sulfur dioxide than the conventional iron-based and nickel-based alloys.[1] They do not corrode readily in sulfur bearing environments because the alloy forms an aluminum oxide coating that resists attack by sulfur. Even if the sulfur should break through, Al_2O_3 reforms rapidly to prevent the propagation of further sulfur attack. The metal filter elements should exhibit greater mechanical reliability in long-term service than the ceramic filters. Although the ceramic materials offer excellent corrosion resistance, they lack fracture toughness and are prone to cracking.

Synthesis of iron aluminide powders and the degradation behavior of the alloy under oxidizing, reducing, and carburizing conditions have been investigated extensively.[1–3] Pall Corporation (Cortland, NY) uses its proprietary process for manufacturing seamless cylinders to fabricate sintered metal elements from water-atomized iron aluminide alloy powders produced by Ametek, Inc. (Eighty Four, PA). The powder is mixed with a water-based solution and a binding agent. The solution is poured into a ceramic preform and rotated to centrifuge the powder and the binding agent to deposit uniformly on the walls of the tube.[4] The preform assembly is dried, isostatically pressed, and vacuum sintered. After the sintering operation, the iron aluminide seamless cylinders are removed from the protective ceramic tubes and are cut to length. Finally, the end fittings of Type 310 stainless steel or solid iron aluminide are welded using a single-pass gas tungsten arc or TIG. The filler can be steel or iron aluminide. Before placing in service, the filter elements are optionally preoxidized in air at 800 °C for 7 h. The preoxidation treatment promotes the formation of a surface enriched in alumina and improves sulfidation resistance.

Cylindrical, sintered metal filter elements of atomic composition Fe-28% Al-2% Cr (FAS) with (FAS-Zr) and without 0.1% Zr were exposed in combustion and gasification conditions in a fluidized bed gasifier/modular gas cleanup rig and in a transport reactor demonstration unit.[5] The filter temperature was 540 to 570 °C and the H_2S concentration was 500 to 8000 ppmv. The tests were of short duration, 100 to 300 h, as the intent was to provide initial guidance on screening materials. Post-test examination of the exposed filters revealed limited corrosion, small (5%) to moderate (33%) reduction in hoop strength, and insignificant degradation of ductility.

The purpose of this study was to investigate the effect of long-term exposure, >2000 h, on the behavior of a high chromium iron aluminide of composition Fe-28% Al-5% Cr (FAL). The alloy of this composition is being considered for field tests, but much of the available data applies to 2% Cr alloys. Whereas the 5% Cr alloy may be suitable for service in both oxidizing and reducing atmospheres, the scope of this work was restricted to a reducing environment containing contaminants from coal gasification: alkali metals, chlorine, sulfur, and ash in the presence of steam. The objective was to characterize the effect of exposure on filtration behavior, filter regenerability, physical and mechanical properties, and microstructure. The tests were done on a subscale filter in a well-controlled laboratory setting with synthetic gases used to simulate the environment of a coal gasifier. Flow-through tests were designed to study the filtration behavior as a function of fluid mechanic variables. A special pulse gas system was assembled to characterize filter regenerability.

Experimental Procedure

Figure 1 shows the experimental apparatus used to expose the metal filter specimens to a controlled reducing gas at 500

V.J. Novick, R.K. Ahluwalia, K. Natesan, W.K. Soppet, and **B.E. Spencer,** Argonne National Laboratory, Argonne, IL 60439-4838. Contact e-mail: natesan@anl.gov.

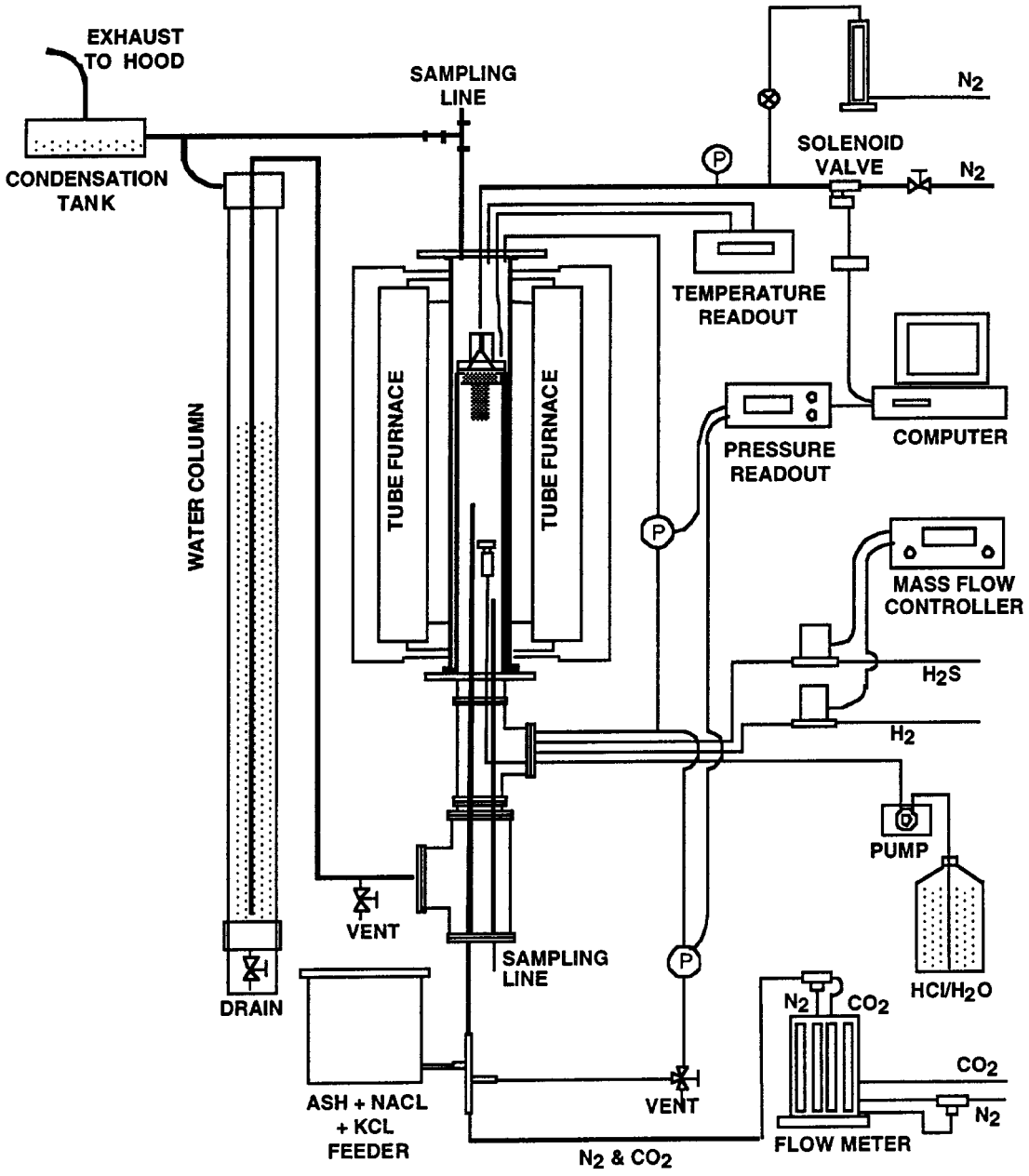

Fig. 1 Filter test apparatus

to 600 °C. It shares many design and construction features with an apparatus used earlier for ceramic filter specimens. These are described in a companion document[6] and will not be repeated here. Suffice it to say that the design allows long duration, unattended, flow-through tests with a provision for on-line, computer-controlled back pulsing to remove the ash captured on the filter. The computer software allows an arbitrary pulse schedule so that the pulse duration, interval, and frequency (single or multiple pulses) are variable; the pressure of the reservoir that supplies N_2 for back pulsing is adjusted manually.

Table 1 lists the composition of the synthetic gases used in the exposure tests. The gas environment was selected to be representative of a pressurized, air-blown, entrained bed gasifier with a desulfurizer upstream of the filter vessel. An exact simulation was not possible because the tests were conducted at atmospheric pressure. As in Ref 6, compressed gas cylinders supplied N_2, CO_2, and H_2S and the reverse water gas shift reaction produced CO. For reasons of reliability, the electrolytic generator was retired in favor of a compressed gas cylinder for H_2. In the first test, HCl was mixed with liquid H_2O, which was aerosolized using a medical inhaler type of an ultrasonic nebulizer. The water mist created by the nebulizer was entrained with CO_2. The acidic solution, however, proved corrosive to the ultrasonic diaphragm and caused repeated failures. The result was that the average amounts of H_2O and HCl in the feed were substantially less than desired. For the second test,

Table 1 Composition of gas used in exposure tests. The equilibrium column is calculated from feed composition and gas phase chemistry

Test conditions	Target	Target equilibrium	Filter 1 (average feed)	Filter 2 (average feed)
CO, %	0	4.3	0	0
H_2, %	17.5	10.7	18	18
CO_2, %	16	11.7	17	16
N_2, %	59	59	61	60
H_2S, %	0.5	0.5	0.5	0.5
H_2O, %	7.5	14.3	3.9	6.1
NaCl, ppm	2	2	1.1	2.4
KCl, ppm	4	4	2.1	4.7
HCl, ppm	40	40	35.8	26.1
Ash, ppmw	5000	5000	1567	5529
Exposure time, h	…	…	1009	2251
Number of cleaning pulses	…	…	1184	2297
Temperature, °C	600	600	600	600
Pressure, atm	1	1	1	1

the nebulizer was replaced by a peristaltic device, which pumped the acidic solution through a 0.32 cm tube near the center of the inner ceramic containment chamber. The liquid solution was heated indirectly by the furnace and vaporized before exiting the 0.32 cm tube. This arrangement allowed the amount of water vapor challenging the second filter to be much closer to the design condition. The drawback was that the resulting pressure transducer signal was noisier because of the water boiling in the injector tube.

The alkali challenge to the filter was in the form of sodium chloride and potassium chloride. It proved convenient to pulverize the crystalline NaCl and KCl and mix them with ash injected into the gas stream. In past tests with ceramic filter specimens, NaCl was dissolved in water fed to the nebulizer.

In earlier test campaigns, a beaded chain transported ash from a reservoir to a chamber, where it was blown off and entrained by a jet of N_2. Adhesion of ash to the chain was found to limit its maximum loading to less than 1000 ppmw. For higher loading, a new arrangement was installed in which a screw drive mechanism conveyed ash from a reservoir to a dispersal chamber. The ash was blown off the end of the screw by a carefully positioned jet of N_2 gas. In the test with the first metal filter, the ash loading was less than 1600 ppmw. Careful diagnostics indicated that the dispersal system was ineffective in that a significant portion of ash was not entrained but deposited on the floor of the chamber, requiring frequent system shutdowns for emptying and cleaning the chamber. In the second test, the chamber was replaced with a much smaller "tee" arrangement that increased the gas velocity. The redesign allowed the ash loading to exceed the 5000 ppmw target.

The ash used to challenge the filters came from the Transport Reactor Demonstration Unit Run number PO47.[4] The composition of the ash analyzed using x-ray fluorescence and x-ray diffraction was 50.4% SiO_2, 20.1% Al_2O_3, 1.4% Fe_2O_3, 0.7% TiO_2, 0.8% P_2O_5, 12.8% CaO, 6.9% MgO, 0.7% Na_2O, and 1.1% SO_3. The average mass median aerodynamic diameter (MMAD) of the dispersed ash measured with an eight-stage cascade impactor was 14.5 μm.

Figure 2 shows the filter specimens, the filter holder, and the back pulse tube. The specimens are 148 mm long, 2 mm thick, and had nominal outer diameter (OD) of 60 mm. The flange is 66 mm in OD and 32 mm in length. The filters are welded to a bottom plate and to the flange. About 141 mm of the filter body is permeable to flow giving a nominal filtration area of 265 cm^2. The test specimen was sealed to the filter holder with a flexible ceramic fiber felt mat, sandwiched between the filter and the collar and the diverter holder assemblies. Separate tests were conducted to ensure that there was no significant leakage around the ceramic mat seal.

Filter Performance

Pressure Drop Behavior

A parametric study was conducted to determine the relationship between ΔP, gas flow rate, and the condition of the filter. Figure 3 presents the data from a series of experiments in which ΔP was measured as a function of N_2 flow rate at a furnace temperature of 600 °C. The open circles represent the data for clean filter 1 and the open squares for clean filter 2. The filled diamonds represent the data for filter 1 after exposure for 480 h to ash and 1000 h to gas. The filled triangles represent the data for filter 2 after 2010 h of ash and 2100 h of gas exposure. The data were taken prior to pulsing after filter 1 was loaded with ash for 1 h and filter 2 with ash for 3 h. The filled circles and crossed squares represent the same total exposure of the filters but with measurements taken after a back pulse. When the ash feeder was operational, the particulate concentration in the gas challenging filter 1 was about 3300 ppmw and that challenging filter 2 was about 6000 ppmw. At a given N_2 flow rate, the difference between prepulse and postpulse data represents the recoverable portion of ΔP due to the ash that accumulates on the filter surface between two consecutive pulses. For stable operation, it should equal the increase of total ΔP between two pulses. The difference between postpulse and clean filter data represents the ΔP offered by the adherent ash cake that is not removed during back pulsing. For operation without a shutdown, this difference should approach an equilibrium value after numerous pulse-cleaning cycles.

The pressure drop data can be reduced by calculating the effective permeability or permeance (k_{eff}) from the Darcy-Forchheimer equation.

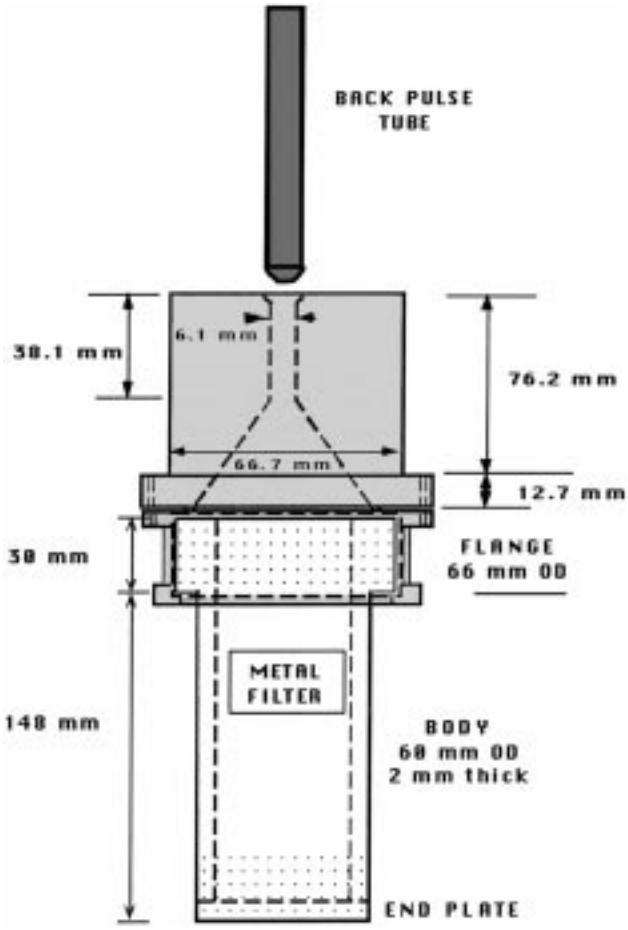

Fig. 2 Filter holder and back pulse system

$$k_{\text{eff}} = \frac{\mu\nu(1 + \text{Re})}{\Delta P}$$

$$\text{Re} = \frac{\beta\rho\nu}{\mu} \qquad \text{(Eq 1)}$$

where ρ is the gas density, μ is the gas viscosity, ν is the face velocity, and β is an empirical coefficient to account for inertial effects. With $\beta = 0$ and data for all combinations of temperature and flow rate included, an average k_{eff} of 0.485 ± 0.064 nm is inferred for clean filter 1 and 0.547 ± 0.065 nm for clean filter 2. These compare with an average k_{eff} of 0.405 ± 0.063 nm for the ceramic fibrosic filters tested under similar conditions.[6] Since it was determined in earlier work that k_{eff} is a function of temperature, further comparisons were limited to 600 °C. The two as-received iron aluminide filters had k_{eff} of 0.569 ± 0.043 and 0.651 ± 0.033 nm, respectively. These compare to k_{eff} of 0.445 ± 0.030 and 0.570 ± 0.019 nm measured for the two ceramic filters at 600 °C. All exposed filters show a marked decrease in permeability due to ash penetration into the pores of the filters and the buildup of residual ash cake on the outer surface. After 1000 h of testing, filter 1 showed a reduced k_{eff} of 0.363 ± 0.047 nm, while filter 2 had k_{eff} of 0.456 ± 0.035 nm after 1778 h and 0.297 ± 0.025 nm after 2251 h of exposure. For comparative purposes, k_{eff} of one of the ceramic filters was

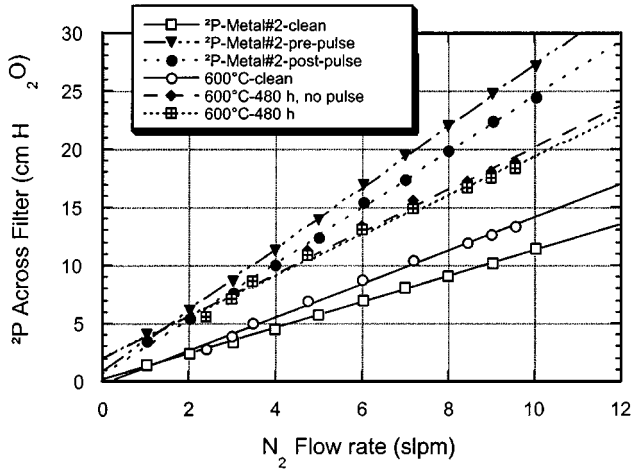

Fig. 3 Pressure drop behavior of filters 1 and 2 before and after exposure

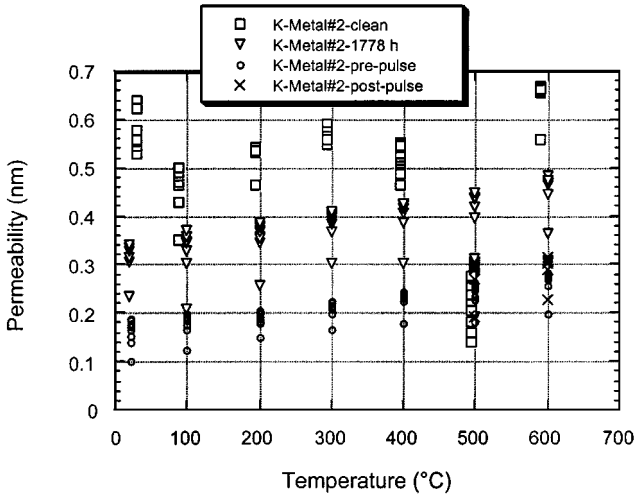

Fig. 4 Derived permeability of the metallic filters as a function of temperature and exposure

calculated to be 0.244 ± 0.023 nm after a 263 h exposure. Figure 4 plots the permeability of the iron aluminide filter 2 as a function of temperature and exposure conditions. The data scatter at a given temperature and condition is due to the different gas flow rates used in the experiments and dependence of k_{eff} on face velocity.

Filter Loading and Cleaning Behavior

As indicated earlier, frequent but intermittent problems with the ash and water feed systems were encountered during the exploratory test with filter 1. These resulted in NaCl, KCl, H_2O vapor, and ash concentrations being much smaller than the target values of 2 ppm, 4 ppm, 7.5%, and 5000 ppmw, respectively. The back pulse pressure was set to 11.4 bar, the pulse duration was 0.5 s, and the filter was cleaned every hour with a single pulse of N_2. For the first 150 h, ΔP increased by 0.75 cm H_2O between the cleaning pulses, and the baseline ΔP rose by about 1.5 cm H_2O. By the end of the 1009 h test, the back

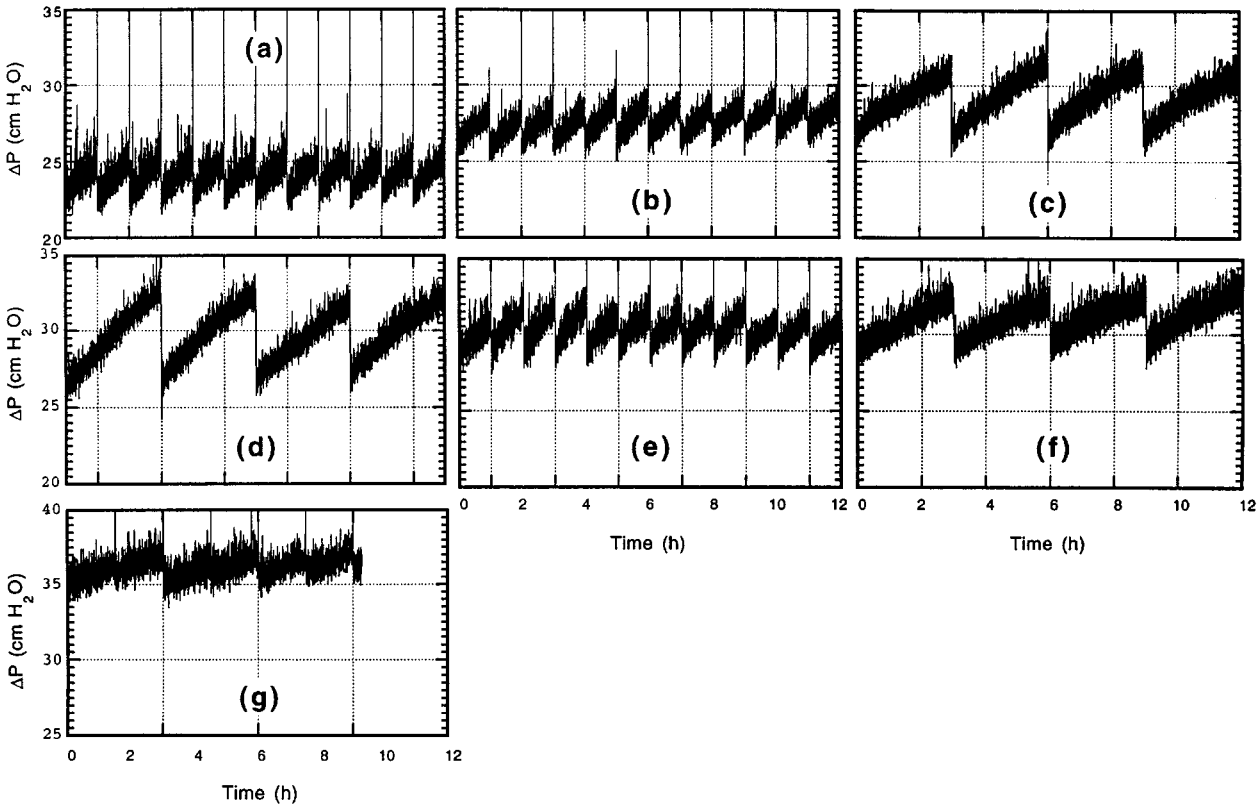

Section of Fig. 5	Temperature °C	Back pressure, bar	Pulse duration, s	Pulse interval, h
a	600	13.6	1	1
b	600	3.4	1	1
c	600	6.8	0.2	3
d	600	6.8	0.1	3
e	600	6.8	0.2	1
f	500	6.8	0.1	3
g	500	3.4	1	1

Fig. 5 Filter regenerability as a function of temperature, reservoir pressure, pulse duration, and pulse interval

pulse pressure had to be raised to 13.4 bar and the baseline *P* had increased by almost 7 cm H_2O.

The ash and water feed problems were corrected for the filter 2 test. The ash feeder was operational for over 94% and the water feed system for more than 81% of the 2251 h total test duration. In addition to improving the efficiency of the dispersal chamber, the ash feed rate was increased. The combination resulted in a 1 h ash loading causing a 3.5 cm H_2O increase in ΔP across the filter. Over the course of the 2251 h test, the baseline ΔP rose by 10 cm H_2O.

Near the end of the filter 2 run, special relatively short duration tests were dedicated to investigating the effects of back pulse parameters on the effectiveness of filter regeneration at 500 and 600 °C. Figure 5(a) and (b) present the data on the effect of reservoir pressure on the ΔP profile. At 600 °C furnace temperature, 1 s pulse duration, and 1 h pulse interval, a stable repetitive saw-tooth profile is established at 14.8 bar reservoir pressure. Under the same conditions, a saw-tooth profile is also evident at 4.5 bar reservoir pressure, but it is nonrepetitive because of the creep in baseline ΔP. There is only a partial recovery in ΔP with each back pulse so that the baseline pressure drop rises from one pulse cycle to the next. Over the course of a 12 h exposure using a 4.5 bar reservoir pressure, the baseline ΔP rises by about 1 cm H_2O.

Figure 5(c) and (d) compare data on filter regenerability as a function of pulse duration at 600 °C furnace temperature, 7.9 bar reservoir pressure, and a 3 h cleaning interval. The data show that a pulse duration of 200 ms is sufficient to repetitively regenerate the filter, whereas the 100 ms pulse duration does not appear to completely restore the filter to the baseline ΔP. For the solenoid valve used in the test apparatus, 18 ms opening, and 30 ms closing time, only pulse durations of 100 ms or longer were tested. After 9 h of operation and three cleaning cycles, the baseline ΔP increased by about 0.5 cm H_2O with 100 ms pulses.

Tests were also run to examine the effect of the pulse interval on filter regenerability. At 600 °C, 7.9 bar reservoir pressure, and 0.2 s pulse duration, the differences in the ΔP traces between 1 and 3 h pulse intervals are evident in Fig. 5(c) and (e) and are considered insignificant. In both cases, the ΔP profiles were

repetitive, the baseline pressures were similar, and the increase in pressure drop between pulses was proportional to the time interval.

Figure 5(f) and (d) demonstrate the combined effect of temperature and back pulse reservoir pressure on the regeneration behavior of the iron aluminide filters. At 7.9 bar reservoir pressure, 0.1 s pulse duration, and 1 h pulse interval, the pressure profiles are similar at 500 and 600 °C. There appears to be no significant difference in filter cleanability, although the baseline pressure drop is higher at 600 °C than at 500 °C. Since the gas flow rates were adjusted to compensate for temperature in order to maintain a filtration velocity of 2 cm/s for both tests, this effect may be due to the difference in gas viscosity. As expected, under the same conditions of pulse duration and interval but 4.5 bar reservoir pressure (Fig. 5g and b), the filters cannot be completely regenerated at 500 or 600 °C. The pressure recovery is less complete, suggesting that the regeneration is even more difficult at 500 °C. It may be that the ash cake characteristics, such as porosity, density, and bond strength, are less favorable at the lower temperature. More tests are required to confirm this inference.

The above results suggest that there is a critical reservoir pressure and pulse duration, below which the iron aluminide candle cannot be regenerated by the simple back pulse technique. Above this critical pressure, a short pulse is as effective in maintaining a stable sawtooth profile as a long pulse, although the baseline pressure may be affected by pulse duration. Pulse schedule, single or multiple pulses, and interval between pulses do not appear to significantly impact filter regenerability. At 7.9 bar reservoir pressure, the required specific flow rate of the pulse gas to clean the filter is 0.32 slpm/cm^2 (standard liter/min/cm^2) of filtration area. Thus, the projected compressed gas consumption for a standard 1500 mm long, 60 mm OD candle is 2 sl/pulse/filter if the pulse duration is 200 ms.

Filter Collection Efficiency

The particle collection efficiency of the iron aluminide filter 1 was measured at three different exposure times. Measurements were taken with a cascade impactor installed in the exhaust line directly above the outlet of the filter holder assembly. The amount collected by the stages of the cascade impactor was compared to mass distribution of the fly ash as dispersed in separate off-line tests of the ash feeder. In addition, the total mass output per unit time of the ash feeder was measured. The average MMAD of the particulates aerosolized by the ash feeder was 14.5 μm. The average output of the ash feeder was 1.14 g/h. The first efficiency test was conducted with the newly installed filter, using only nitrogen gas at a flow rate of 10.2 slpm. The total collection efficiency based on the mass collected downstream of the filter and the estimated mass challenging the filter was determined to be 99.71% for the TRDU ash. A second test was conducted after 840 h of exposure to ash, alkali, and simulated combustion gases. Impactor measurements indicated that the filtration efficiency had improved to 99.89%. A final test was conducted at the end of the 1009 h test. The final filtration efficiency for the iron aluminide filter was measured to be 99.96%. The improvement in efficiency with increased exposure is a common phenomenon, attributed to the added filtration provided by the ash cake formed on the surface of the filter. Analysis of the cascade impactor and ash feeder data show a minimum collection efficiency of 99.78% for particles larger than 16 μm, 99.70% for particles between 7.85 and 16 μm, 99.70% for particles between 4.24 and 7.85 μm, 99.62% for particles between 2.05 and 4.25 μm, 99.34% for particles between 1.09 and 2.05 μm, 98.78% for particles between 0.66 and 1.09 μm, and 98.78% for particles between 0.40 and 0.66 μm.

Ash Cake Characterization

Post-test examination of the exposed filters revealed nearly uniform coating of the residual ash on both filters. Filter 1 was removed from the test stand after a final cleaning pulse. The filter 1 cake is termed permanent, since it was not removed with back pulse of gas. The ash cake was scribed and photographed under low magnification. The cake thickness, determined by the depth of the scribe mark, was measured to range from 0.0569 to 0.0772 cm with an average of 0.0624 $\pm$ 0.0166 cm. The mass of the cake scraped form the surface was 3.86 g. Using the measured bulk ash density of 1.142 g/cm^3 and a cake density of 0.229 g/cm^3, a void fraction of 80% was inferred. The weight difference between the clean filter and the scraped filter was 1.58 g. The majority of this mass is attributed to ash penetration into the interstitial regions of the filter. Some mass change may also be due to the formation of the corrosion products on the filter.

Filter 2 was removed from the test stand with 3 h of entrained ash loaded onto the filter after the last back pulse. The total ash deposit measured in this way should correspond to the combination of the permanent cake plus the cleanable ash from the last 3 h of loading. The combined thickness of the permanent and removable ash cakes was optically determined to range from 0.224 to 0.322 cm with an average over the entire surface of 0.270 $\pm$ 0.04 cm, based on pretest and post-test measurements of the filter diameter. The total mass of ash removed from the filter surface was 14 g. Based on the average feed rate for the entire test, 11.6 g of ash would be loaded in 3 h. This implies that if all of the ash fed into the system reached and was collected by the filter surface, the permanent cake would be on the order of 2.4 g. The difference in mass between the scraped filter and the initial clean filter was 1.31 g.

The permanent cake can also be estimated as the difference between the final filter weight and an earlier weight that included a permanent cake formed after about 1800 h of operation. The weight at 1800 h was obtained during a temporary shutdown and disassembly, necessitated by a break in the ceramic tube used for containment. This mass difference, representative of the amount of ash loaded in 3 h plus any additional to the permanent cake in the last 400 h, was found to be 10.41 g. The permanent cake mass can be calculated by subtracting this gain plus the mass of ash imbedded in the filter, from the scraped mass. This difference is 2.28 g, which is in good agreement with the 2.4 g calculated on the basis of the ash feed rate. The differences in the permanent ash cakes between filters 1 and 2 may be due to the difference in the total amounts of water, alkali, and H_2S passing through the respective cakes.

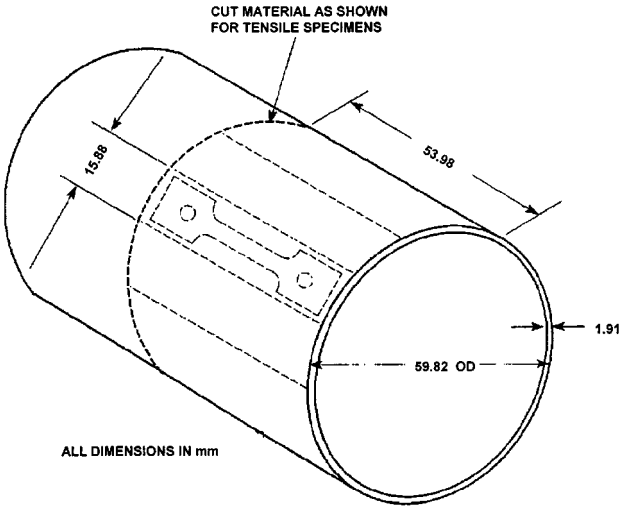

Fig. 6 Orientation and geometry of tensile specimens

Corrosion and Mechanical Performance

Upon completion of the two long duration tests, the tube specimens were analyzed in detail for their residual mechanical properties and microstructural characteristics, especially from the standpoint of corrosion.

Tensile Tests

Uniaxial tensile specimens were fabricated from the as-received filter tube and from the exposed filters 1 and 2. Tensile specimens were cut in the axial direction of the tube, as shown in Fig. 6. The specimens were fabricated according to ASTM specifications and had a gauge length of 1.9 cm and a gauge width of 0.45 cm. In some of the specimens, both sides of the gauge lengths were machined flat, while in some, only the ID side of the specimen was machined in order to maintain the OD surface (that was exposed to the dirty gas side) intact in the as-exposed condition. Tensile tests were conducted at room temperature (25 °C) and 600 °C at a strain rate of 1.7×10^{-4} s^{-1}. Tests at room temperature were conducted in ambient air and those at 600 °C were conducted in a vacuum environment. The specimens were loaded by means of pins that pass through holes in the grips and the enlarged end sections of the specimen, thus minimizing misalignment.

Total elongation, measured with vernier caliper and load/elongation chart records, is reported as a ratio of the length increase to the original length of the specimen. The maximum engineering stress, uniform elongation, and total elongation for specimens with various treatments are listed in Table 2. Fracture locations, listed in Table 2 for various specimens, indicate that the porous nature of iron aluminide filter material is susceptible to inherent flaws, which lead to fracture of several specimens close to the shoulder regions of the machined samples. Locations labeled "GL" were fractures that occurred in roughly the middle third of the specimen. Fractures labeled "End of GL" occurred at the radius portion of the specimen.

Figure 7 shows the variations in maximum engineering stress at room temperature and at 600 °C for the filter material in the as-received condition (AR) and after exposure for filter 1 (EX) and filter 2 (EX2). The letters D and E in tensile specimen identification (*e.g.*, D01 and E01) correspond to specimens that were machined on both sides (D) and those on the ID side only (E). Results indicate that the maximum engineering stress at 600 °C in vacuum is in the range of 55 to 69 MPa, irrespective of exposure to environments used in the present study.

Figure 8 shows the variations in uniform and total elongation at room temperature and at 600 °C for the filter material in the as-received condition and after exposure. At room temperature, the elongation is less than 0.2%, indicating the brittleness of the material. At 600 °C, the uniform and total elongations for the material are 1% and 3%, respectively, and are essentially the same before and after exposure to the test environments.

Four-Point Bend Tests

Four-point bend tests were performed on the iron aluminide filter material in the as-received condition and after exposure. Tests were conducted at room temperature in ambient air and at 600 and 650 °C in a vacuum environment. Four-point bend specimens were fabricated from the tube sample in the orientation depicted in Fig. 9. The specimens were of dimensions 2.54 $\times$ 0.475 $\times$ 0.16 cm, machined on all sides.

The load to cause fracture measured in the test is used to calculate the flexural strength for the materials using the expression

$$\sigma = \frac{3(L_1 - L_2)P}{2t^2w} \qquad \text{(Eq 2)}$$

where σ is flexural strength, L_1 is the distance between the support points, L_2 is the distance between the load points, P is the load, and t and w are the thickness and the width of the specimen, respectively. The testing technique produces a non-uniform stress distribution with the maximum tensile stress in the outer skin of the specimen. Figure 10 shows the maximum load obtained at room temperature, 600, and 650 °C for specimens with various treatments. The results indicate a slight decrease in maximum load for the material after exposure in the test environment. Figure 10 also shows the variation in absorbed energy at the point of maximum load and total energy for specimens with various treatments. At room temperature, the absorbed energy at maximum load and total energy are almost the same, indicating a sharp catastrophic fracture of the specimens. Furthermore, the absorbed energy values are 1 to 2 J/cm^2, indicating brittleness of the material at room temperature. At elevated test temperatures, the absorbed energy values were in the range of 4 to 9 J/cm^2, and the total energy values were 8 to 15 J/cm^2.

Also included in Fig. 10 is a bar graph of the "ductility index" (defined as the absorbed energy subsequent to maximum load as a fraction of total energy) for specimens with various treatments. The results indicate that the index is negligibly small for the material tested at room temperature, indicating the brittleness of the material. The data show some improvement in ductility index at elevated temperatures, but the results are not sufficient to quantify the effects from the standpoint of exposure environment and test temperature.

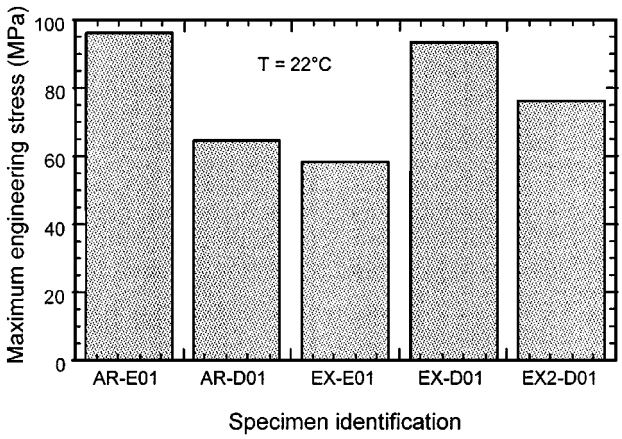

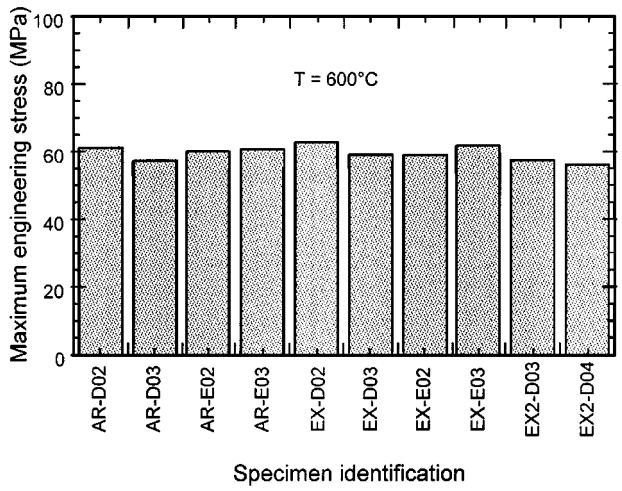

Fig. 7 Maximum engineering stress of the as-received and exposed iron aluminide filter material at room temperature and at 600 °C

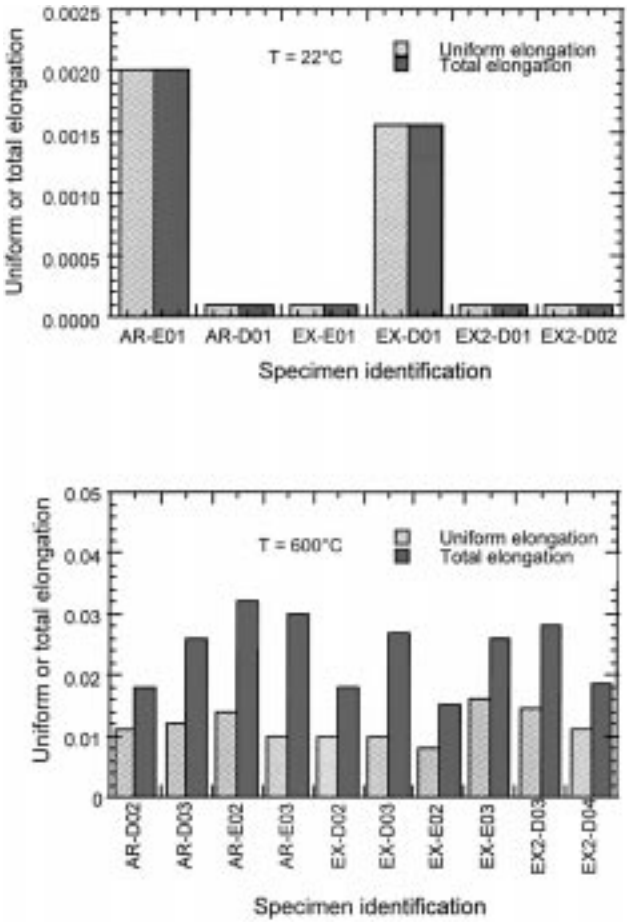

Fig. 8 Uniform and total elongation of the as-received and exposed iron aluminide filter material at room temperature and at 600 °C

Table 2 Stress and elongation data for iron aluminide filter specimens tested

Test number	Specimen number	Test temperature (°C)	Max. eng. stress (MPa)	0.2% yield stress (MPa)	Uniform elongation	Total elongation	Test atmosphere	Fracture location
FeAl-01	AR-E01	25	96.0	89.6	0.0020	0.0020	Air	End of GL
FeAl-02	AR-D01	25	64.6	…	0.0001	0.0001	Air	End of GL
FeAl-03	EX-E01	25	58.1	…	0.0001	0.0001	Air	GL
FeAl-04	EX-D01	25	93.3	…	0.0016	0.0016	Air	GL
FeAl-13	EX2-D01	25	76.2	…	0.0001	0.0001	Air	End of GL
FeAl-14	EX2-D02	25	65.6	…	0.0001	0.0001	Air	End of GL
FeAl-05	AR-D02	600	61.4	56.8	0.0110	0.0180	Vacuum	End of GL
FeAl-08	AR-D03	600	57.0	52.7	0.0120	0.0260	Vacuum	End of GL
FeAl-11	AR-E02	600	59.9	54.9	0.0140	0.0320	Vacuum	End of GL
FeAl-12	AR-E03	600	60.8	57.6	0.0100	0.0300	Vacuum	GL
FeAl-06	EX-D02	600	62.7	58.8	0.0100	0.0180	Vacuum	GL
FeAl-07	EX-D03	600	59.2	54.8	0.0100	0.0270	Vacuum	End of GL
FeAl-09	EX-E02	600	58.8	55.8	0.0080	0.0150	Vacuum	End of GL
FeAl-10	WX-E03	600	61.7	52.6	0.0160	0.0260	Vacuum	End of GL
FeAl-15	EX2-D03	600	57.3	51.0	0.0146	0.0282	Vacuum	End of GL
FeAl-16	EX2-D04	600	56.3	51.6	0.0110	0.0184	Vacuum	End of GL

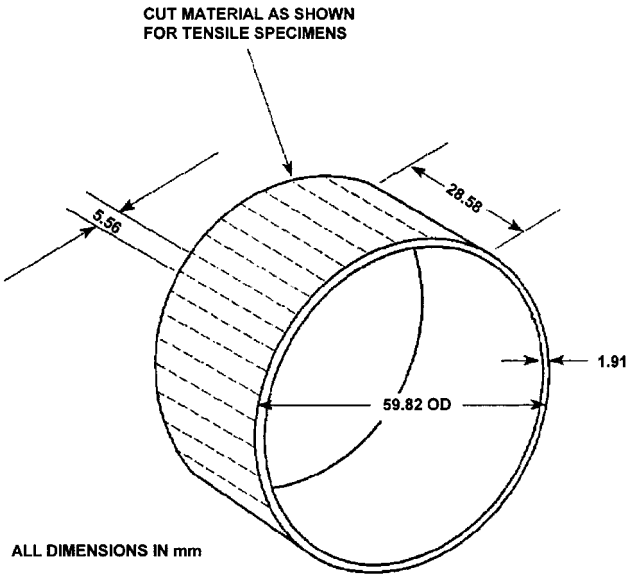

Fig. 9 Orientation and geometry of specimens used in four-point bend tests

Microstructural Analysis

The filter tubes were analyzed in detail to evaluate the effects, if any, of exposure environment on the corrosion performance of the porous alloy. These filters are preoxidized to create a passive layer of alumina, which helps increase resistance to sulfur containing atmospheres. Sections were cut from the as-received and the exposed filters. These filter specimens were examined using a scanning electron microscope (SEM) equipped with an energy-dispersive x-ray (EDX) analyzer. Figure 11(a) is an SEM photo of clean, untested filter to provide a reference for later comparison with exposed filters. Numerical markers on the micrograph denote areas where x-ray analysis was conducted. Table 3 provides the elemental EDX analysis for the clean filter. Region 6-1 indicates localized areas of higher iron content and the lower level of aluminum denotes a thinner layer of alumina coating. Regions 6-2 and 6-3 exhibit a similar composition throughout the bulk of the filter.

Figure 11(b) shows the outside surface of a filter specimen (250×) after exposure to the conditions of the first 1009 h test. Table 3 provides the EDX measurements corresponding to the numerical markers in Figure 11(b). The white areas (7-1 and 7-3) appear to be mostly lower density compounds, probably caused by corrosion and ash buildup, and exhibit low iron content. A nodule of ash in region 7-4 is indicated by high calcium, silicon, and oxygen content. The darker areas, exemplified by region 7-2, exhibit iron concentrations consistent with the unexposed filter EDX data from Table 3.

Figure 12 shows the micrographs of the inner and outer surfaces of the metal filter specimens from filter 1 that exhibited areas of visual corrosion. In general, filter 1 experienced local attack, which showed as a black corrosion product on the outer surface of the filter tube; however, except for this locally black region, most of the filter surfaces seemed to have undergone only slight general oxidation. The SEM analysis was made of the black (heavily corroded) region and an area with normal oxidation.

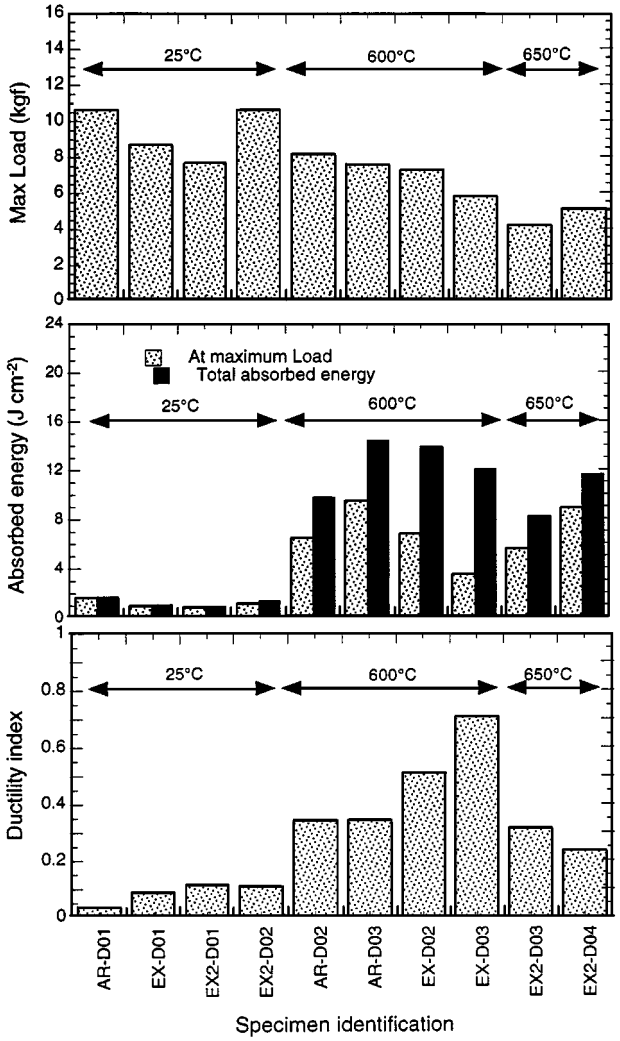

Fig. 10 Maximum load, absorbed energy, and ductility index of the as-received and exposed iron aluminide filter material at room temperature, 600 °C, and 650 °C

Figure 13(a) and (b) are the SEM photomicrographs (100× magnification) and elemental mapping for Al, S, O, Cr, and Fe for corroded regions in the vicinity of the ID and OD surfaces, respectively, of exposed filter 1.

The EDX analysis was conducted on the cross section of the high corrosion area, specifically measuring the concentration of sulfur along four different paths from the outer to inner surface of the filter specimen. The measurements were taken at a magnification of 370×, in 100 μm increments through the cross section. Figure 14 plots the weight percent of sulfur as the filter 1 cross section is traversed from the outer surface to the inner surface. Note that two paths show no sulfur corrosion throughout the cross section, and two paths show significant sulfur corrosion in the first 800 μm of the outer surface. One of the latter paths also indicates some corrosion on the inner surface of the filter to a depth of about 600 μm.

It is evident that a substantial penetration of sulfur had occurred from both surfaces into the interior of the filter wall. The morphology seems to indicate that the sulfur is associated

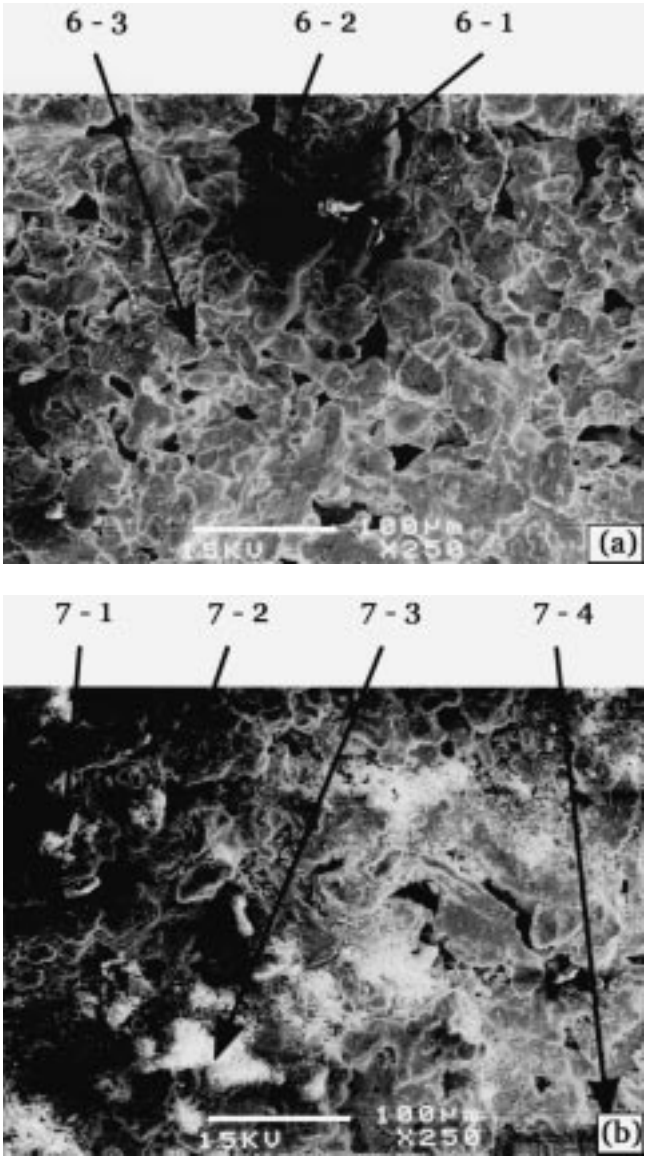

Fig. 11 SEM micrographs (250×) of the outside surfaces of the (a) as-received and (b) exposed iron aluminide filters

Table 3 X-ray analysis of regions labeled in Fig. 11

Element	6-1	6-2	6-3	7-1	7-2	7-3	7-4
Oxygen	1.62	2.43	8.86	41.59	13.86	41.35	20.66
Aluminum	4.57	35.56	32.47	10.35	34.74	7.36	5.58
Sulfur	0	0.18	0	1.02	0	1.14	4.17
Chlorine	0	0.17	0	0.72	0	0.36	0
Chromium	6.59	4.63	6.56	0.85	5.15	0.6	0.3
Iron	86.96	54.49	51.9	16.12	46.25	4.5	7.91
Calcium	0	0	0.2	18.85	0	21.12	18.52
Magnesium	0	0	0	3.5	0	7.94	1.24
Silicon	0.27	2.54	0	7	0	15.63	41.56

with Fe and the corrosion product phase is probably FeS. The results show that protectiveness of the alumina scale that develops in the exposure environment at 600 °C is thin and fragile and can be locally breached, possibly during the pulsing mode of operation of the filter. It is also possible that the thin alumina layer may have spalled and removed with the filter cake material, thereby exposing iron to locally sulfur enriched gas environment. Since alumina growth rates, especially at 600 °C, are extremely slow, formation of FeS is a distinct possibility. In fact, in one micrograph of the inner surface of a specimen, definite evidence of crystallization was observed. The EDX analysis of the crystal area indicated that iron accounts for 49% and sulfur accounts for 34% of the material observed, resulting in the conclusion that the crystals are iron sulfide. Sulfidation attack is an irreversible process in the sense that, even if the sulfides are reoxidized, the sulfur that is released during reoxidation will be driven into the material, which can eventually result in a decrease in porosity of the filter or embrittlement of the material.

Figure 13(c) and (d) show the regions of the same filter (exposed in the first test) that exhibited normal oxidation. No sulfur was detected on either surface, indicating that the material, if protected by even a thin layer of adherent alumina, can offer resistance to attack by sulfur. Figure 13(e) and (f) are the SEM photomicrographs (100× magnification) and elemental mapping for Al, S, O, Cr, and Fe for the filter material in the vicinity of the ID and OD surfaces, respectively, after exposure for filter 2. Even though this run was of much longer duration, no localized attack is observed. Sulfur was detected on both the ID and OD sides of the filter, but it was confined to the surface only and did not penetrate into the interior of the filter wall.

Porosimetry Data

A Micromeritics Pore Sizer 9310 (Micromeritics, GA) was used for porosimetry measurements on two samples each of as-received filter for control purposes, the filter subjected to both the nominal 1000 h test and the nominal 2000 h test. Table 4 summarizes the data for the porosimetry tests. Note that subjecting an iron aluminide filter to the reducing gas conditions described earlier appears to have no effect on the bulk density and little or no effect on the skeletal density of the filter. The corrosive gas appears to cause an increase in the average pore size and a small increase in the measured open fraction of the filter material. The increase in pore size and open volume fraction in the filter means that the ash particles, which have approximately the same diameter as the pores, do not appear to penetrate the interstitial regions of the filter, and hence, do not result in reduced open volume fraction or smaller average pore sizes.

Summary and Conclusions

Two high chrome iron aluminide filters of nominal composition Fe-28% Al-5% Cr have been exposed to a reducing gas environment for 1000 and 2251 h. The data obtained in the tests support the following conclusions concerning filtration behavior, regenerability by reverse pulse gas cleaning, mechanical properties, and microstructural stability.

- The seamless cylinder fabrication method produces metal elements with 33.7 ± 2.40% porosity, 10.77 ± 0.04 μm

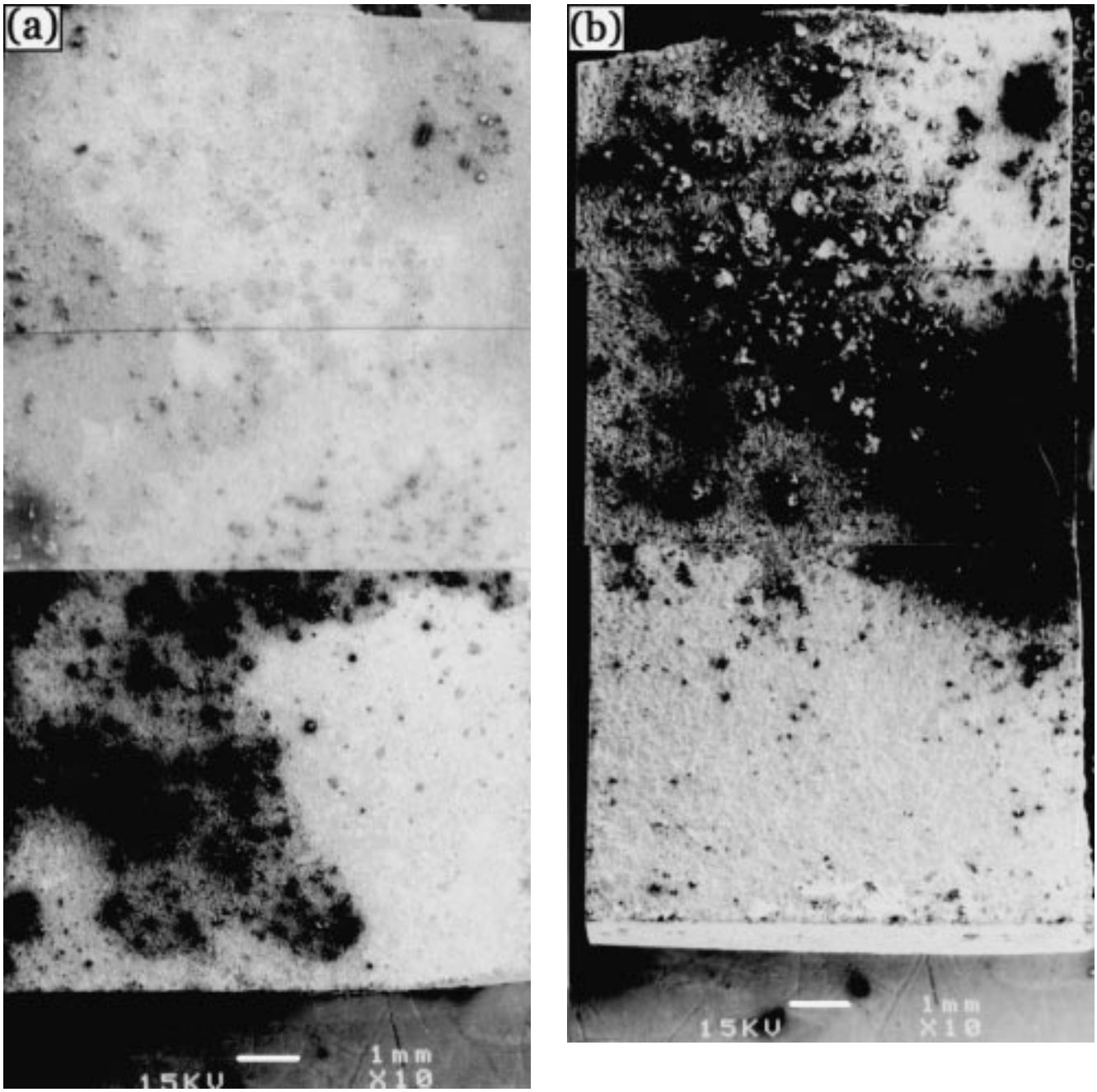

Fig. 12 SEM micrographs (10×) of the (a) outer and (b) inner surfaces of specimens from filter 1 that exhibited visual corrosion

Table 4 Porosimetry data for as-received and exposed filters

	New-1	New-2	1000 h-1	1000 h-2	2000 h-1	2000 h-2
Median pore diameter (μm)	10.80	10.73	11.62	12.55	11.55	11.79
Bulk density (g/cm^3)	3.81	3.87	3.81	3.9	3.81	3.9
Skeletal density (g/cm^3)	6.17	6.37	5.88	6.13	6.16	6.26
Void fraction (%)	31.3	36.1	37.4	36.9	40.5	36.6

median pore diameter, and 3.84 ± 0.03 g/cm^3 bulk density. After 2251 h exposure to the reducing gas environment, the median pore diameter increased slightly to 11.67 ± 0.12 μm and the porosity to 38.55 ± 1.95%.

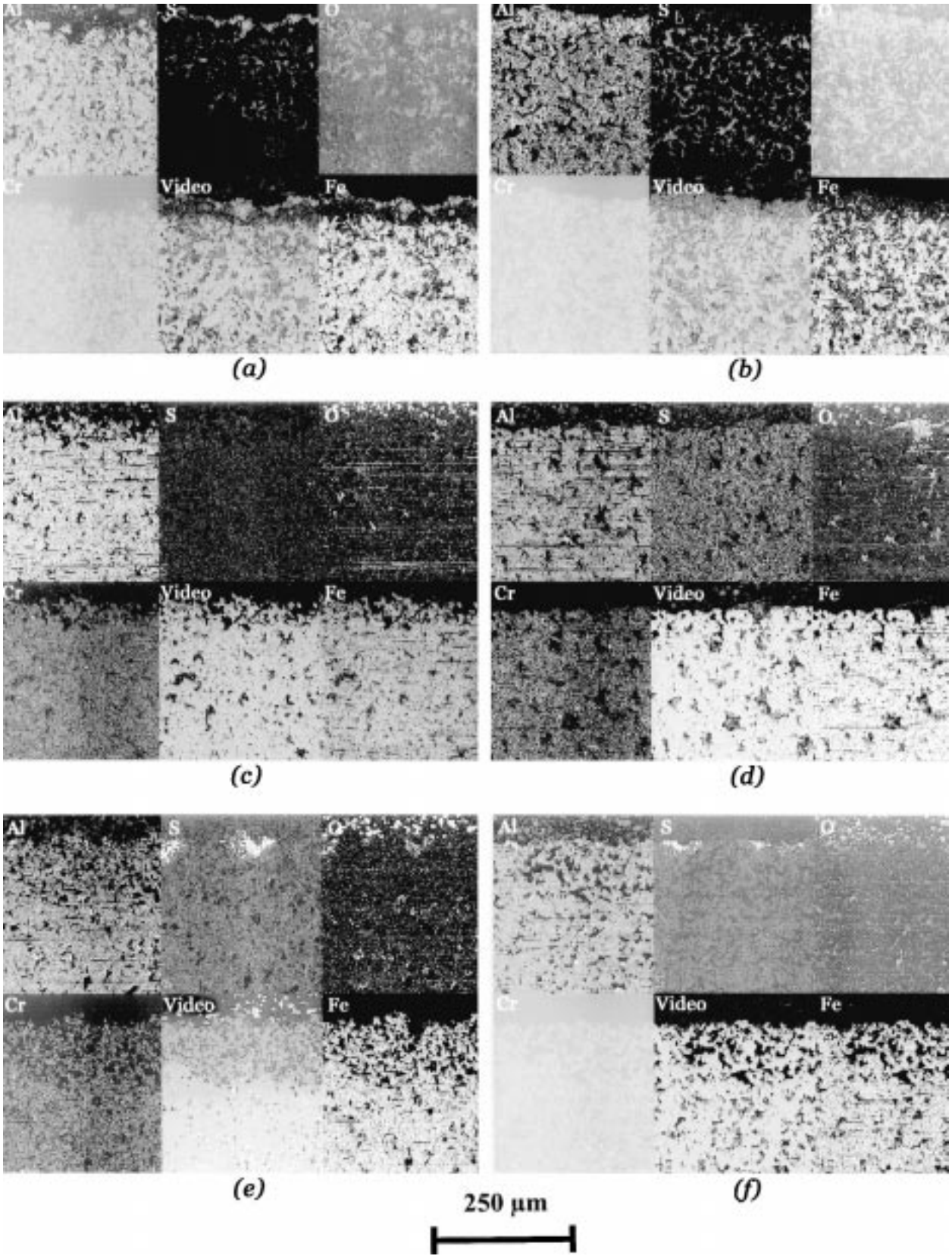

Fig. 13 SEM micrographs and elemental mapping for Al, S, O, Cr, and Fe: (a) corroded region on ID side of exposed filter 1; (b) corroded region on OD side of exposed filter 1; (c) noncorroded region on ID side of exposed filter 1; (d) noncorroded region on OD side of exposed filter 1; (e) ID side of exposed filter 2; and (f) OD side of exposed filter 2

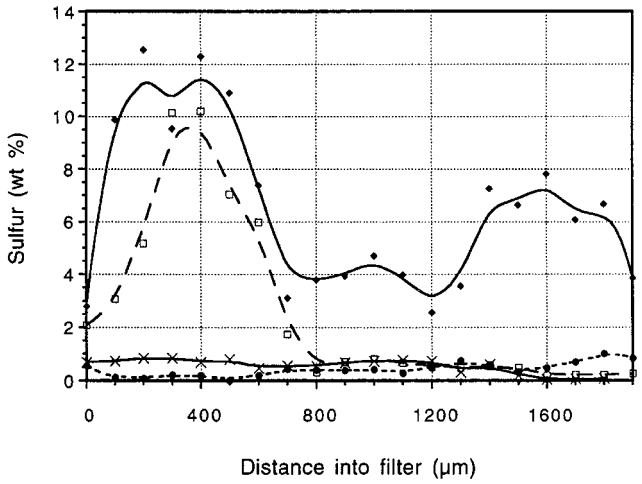

Fig. 14 Profile of elemental sulfur penetration for four different paths from outer to inner surface of exposed filter 1

- The sintered metal filter elements have adequate permeability. At room temperature, the asreceived metal filters show a pressure drop of 41.5 cm H_2O/slpm/(m^2 filtration area), which increases to 52.8 cm H_2O/slpm/(m^2 filtration area) at 600 °C.
- After exposure to TRDU ash, an ash cake builds upon the filter surface that contributes an additional pressure drop of 52.8 cm H_2O/slpm/(m^2 filtration area) at 600 °C. The ash cake is regarded as permanent in that it is not removed by periodic gas pulsing. At steady state, the residual cake was 2.7 mm thick and had a density of 0.229 g/cm^3 and a void fraction of 80%.
- The sintered metal filter can be successfully regenerated by reverse gas pulsing. According to the experimental data, the minimum pressure to maintain a stable saw tooth profile is 7.9 bar and the minimum pulse duration is 200 ms. The projected pulse gas consumption is 0.32 sl/(m^2 filtration area)/pulse.
- The as-received sintered metal elements show a filtration efficiency of 99.89% for ash particles with MMAD of 14.5 μm. With a permanent 2.7 mm ash cake in place, the efficiency improves to 99.96%.
- In tensile tests, the 5% Cr material shows 58 to 96 MPa maximum engineering stress at room temperature and 55 to 65 MPa at 600 °C. There was no significant deterioration in tensile strength with 2251 h exposure to reducing gas containing sulfur.
- The iron aluminide material containing 5% Cr exhibits brittle behavior in tensile tests at room temperature. The measured uniform and total elongation was less than 0.2% at 25 °C. The material becomes somewhat ductile at 600 °C with the uniform elongation increasing to 1% and total elongation to 3%. The measured elongation is unaffected by exposure to the test environment.
- Four-point bend tests confirm that the material is brittle at room temperature. It exhibits a sharp catastrophic fracture: the absorbed energy at the maximum load and the total energy are nearly the same, 1 to 2 J/cm^2. At 600 °C, the absorbed energy at the maximum load improves to 4 to 9 J/cm^2 and the total energy to 8 to 15 J/cm^2.
- The material is stable under the reducing environment when tested, although scanning electron microscopy did reveal some localized sulfidation attack. The morphology indicates that the sulfur is associated with iron and the corrosion product phase is possibly FeS. It appears that the alumina scale that develops in the exposure environment at 600 °C is thin and fragile and can be locally breached during pulse cleaning, However, the majority of the filter surface undergoes simple oxidation with no visible sulfur. The material, if protected by a thin layer of adherent alumina, can offer resistance to attack by sulfur.

Acknowledgments

This research was sponsored by the U.S. Department of Energy's Federal Energy Technology Center. Dr. N. Holcombe was the Contracting Office Representative. The filter specimens were fabricated by Pall Corporation. We thank R. Haglund and V. Em-Udom for their assistance in operating the filter test stand and D.L. Rink for assistance in the SEM and EDX analyses. The submitted manuscript has been authored by a contractor of the U.S. Government under Contract No. W-31-109-ENG-38. Accordingly, the U.S. Government retains a nonexclusive, royalty-free license to publish or reproduce the published form of this contribution, or to allow others to do so, for U.S. Government purposes.

References

1. K. Natesan: *Mater. Sci. Eng. A,* 1998, vol. A258, p. 126.
2. K. Natesan and P.F. Torterelli: *Proc. Int. Symp. on Nickel and Iron Aluminides: Processing, Properties, and Applications,* Cincinnati, OH, Oct 7–9, 1996, ASM International, Materials Park, OH, 1997, p. 265.
3. P.F. Torterelli, C.G. McKamey, E. Lara-Curzio, B.A. Pint, I.G. Wright, and R.R. Judkins: *Proc. Advanced Coal-Based Power and Environmental Systems '98 Conf.,* Pittsburgh, PA, 1998.
4. J. Hurley, S. Brosious, and M. Johnson: *Proc. Advanced Coal-Fired Power Systems Review Meeting,* Morgantown, WV, July 1996.
5. R.R. Judkins, P.F. Torterelli, and I.G. Wright: *Proc. Advanced Coal-Fired Power Systems Review Meeting,* Morgantown, WV, July 1996.
6. R.K. Ahluwalia, V.J. Novick, L. Zhang, M.P. Sutaria, and J.P. Singh: *ASME J. Eng. Gas Turbines Power,* 2001, vol. 123, pp. 293-302.